

Engineering multifunctionality at oxide interfaces by multimode coupling

Monirul Shaikh and Saurabh Ghosh*

Department of Physics and Nanotechnology, SRM Institute of Science and Technology, Kattankulathur - 603 203, Tamil Nadu, India

We employed first-principles density functional theory calculations guided by group-theoretical analysis and demonstrated the control of insulator-metal-insulator transition, polarization and two sublattice magnetization in $(\text{LaFeO}_3)_1/(\text{CaFeO}_3)_1$ superlattice via. multi structural mode coupling i.e., 'multimode coupling'. We have discovered a polar A-type charge disproportionation mode, Q_{ACD} (analogous to the A-type antiferromagnetic ordering), and found that it couples with the trilinear coupling, Q_{Tri} mode (common in $Pnma$ perovskite oxides and involves three structural modes), and lowers the symmetry further. By tuning the strength of the coupling between the participating modes, the polar metallic phase, polar zero bandgap semiconducting, and polar insulating phases can be obtained. Here, Q_{Tri} switches the polarization direction, whereas, Q_{ACD} can trigger insulator-metal-insulator transition along with the polarization switching. The mechanism is true for any transition metal superlattices constituted with $Pnma$ building blocks and with partially filled e_g or t_{2g} electron(s) at the transition metal sites.

Mode coupling in real materials not only drives structural phase transition but also drives functional properties into the low symmetry phase. The ABO_3 perovskite oxides are among the most studied systems owing to their functional properties such as ferroelectricity, weak ferromagnetism, linear magnetoelectricity and many other, primarily driven by structural distortions [1–5]. In $Pnma$ ABO_3 oxides, the trilinear coupling, $Q_{Tri} \sim Q_T \otimes Q_R^+ \otimes Q_{AFEA}$, between tilt (Q_T) and in phase rotation (Q_R^+) of BO_6 octahedra and anti-ferroelectric A-site displacement (Q_{AFEA}) mode is responsible for driving the phase transition. By employing layered ordering at the A-site, i.e., by constructing AO and A'O layer, the anti-ferroelectricity can be tuned into ferroelectricity leading to finite polarization into the system. Here, Q_T and Q_{R^+} drive weak ferromagnetism and linear magnetoelectricity, respectively, into the system and the polarization is induced by the trilinear coupling [6, 7]. This is known as the hybrid improper ferroelectric (HIF) mechanism [5] which is one of the most successful paradigms in designing multiferroic materials where more than one ferroic property can coexist and cross coupled [6–12].

Apart from common distortions a certain type of structural distortion, termed as a charge disproportionation mode (Q_{CD}) has a deterministic role in obtaining insulator-to-metal transition (IMT) [13]. The Q_{CD} mode is mainly observed in systems those contain charge orderings at the B-sublattice [13–18], e.g., perovskite CaFeO_3 [14, 19]. In CaFeO_3 , electronic phase separation is associated with a charge disproportionation, $2d^{4+} \rightarrow d^{5+} + d^{3+}$, which is responsible for the band gap opening [14, 19]. Similar mechanism follows for other IMT based materials. In this context, it is proposed that the charge disproportionation and hence the IMT transition can be driven by the intermixing of transition metal ions at the oxide interface and that also can happen in

the presence of the polar distortion [20]. Further, perturbation, like strain, tunes the local bonding environment leading to the modification of the band structure at the Fermi level [21].

In this paper, within $(\text{LaFeO}_3)_1/(\text{CaFeO}_3)_1$ superlattice (SL) with C-type magnetic configuration, we report a new type of polar charge disproportionation mode Q_{ACD} , as here, the charge disproportionation has A-type ordering (in analogy with A-type magnetic orderings). We show a multimode coupling, $Q_M \sim Q_{Tri} \otimes Q_{ACD}$ exists between Q_{Tri} and Q_{ACD} , which lowers the energy with a lower space group (Pc) as compared to the trilinear coupling, Q_{Tri} , in perovskite SLs (i.e., $Pmc2_1$) [22]. The electric polarization (\mathbf{P}), magnetization (\mathbf{M}) and IMT show strong correlation and can be tuned via. strain by modifying the strength of the coupling leading to polar metallic, polar zero bandgap semiconducting, and polar insulating phases. Interestingly, the Q_{ACD} is found to switch the direction of polarization of the system through an insulator-metal-insulator path and orbital ordering plays a pivotal role. Finally, we demonstrated that beyond conventional understanding, the mode coupling at the interface and emergence of associate multifunctionality is applicable for any layered $(\text{ABO}_3)_1/(\text{A}'\text{B}'\text{O}_3)_1$ SLs of transition metal oxides (TMOs) with $Pnma$ symmetry and with unpaired e_g or t_{2g} electrons.

Density functional theory (DFT) [23] calculations are performed for total energy, geometry optimization and electric polarization using the Berry phase method [24] as implemented VASP [25]. The K-integration in the Brillouin zone is performed using Γ -centered $6 \times 6 \times 4$ points using 500.0 eV energy cut-off. We considered the generalized gradient approximation (GGA) augmented by the Hubbard-U corrections (GGA+U) [26, 27] to describe exchange-correlation effects. To consider d - d Coulomb interactions, we employed U parameters of 5.0, 3.5, 3.0,

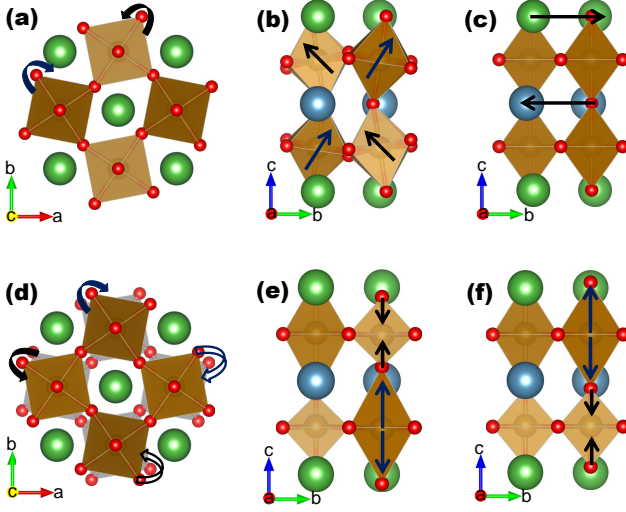


FIG. 1. (a) In-phase rotation, $a^0a^0c^+$ (Q_R^+ , irrep. M_2^+); (b) Tilt $a^-a^-c^0$ (Q_T , irrep. M_5^-); (c) Anti-ferroelectric A-site displacement (Q_{AFEA} , irrep. Γ_5^-), (d) Out-of-phase rotation, $a^0a^0c^-$ (Q_R^- , irrep. M_4^-), (e) Charge disproportionation mode analogous to the G-type anti-ferromagnetic ordering (Q_{GCD} , irrep. M_2^-); and (f) Charge disproportionation mode analogous to the A-type anti-ferromagnetic ordering (Q_{ACD} , irrep. Γ_3^-). The curved arrow with blue (black) is the eye-guide for rotation of FeO_6 octahedra in a clock-wise (counter clock-wise) direction. The shape-filled (unfilled) curved arrow highlight the top (bottom) layer rotation of the FeO_6 octahedra.

1.0 eV for the Fe- d , Cr- d , Ru- d , Nb- d respectively, and 4.0 eV for Mo- d and Mn- d electrons, while the intra-atomic Hund's exchange parameter J is kept as 1.0 eV [9]. The exchange-correlation part is estimated by PBEsol functional [28]. The total energy and Hellman-Feynman force are converged to 0.01 meV and 1 meV/Å, respectively.

We have performed phonon calculations on high symmetry $P4/mmm$ structure of $(\text{LaFeO}_3)_1/(\text{CaFeO}_3)_1$ SL to get insights into stable and unstable structural modes (see Supplementary Note: I and II for more details). The participating modes that drive the HIF are shown in Figure 1 at the top panel. The in-phase rotation Q_R^+ ($a^0a^0c^+$) and tilt Q_T ($a^-a^-c^0$) are as shown in Figure 1(a) and (b), respectively. The third structural distortion, i.e., anti-ferroelectric A-site displacement mode is shown in Figure 1(c). In addition to the HIF modes, we found other three important structural modes. These are out-of-phase rotation Q_R^- ($a^0a^0c^-$) where the in-plane oxygen atoms of FeO_6 octahedra in the two successive layers are rotating in the opposite directions as is shown in Figure 1(d). The charge disproportionation mode analogous to the G-type anti-ferromagnetic configuration (hereafter Q_{GCD}) as shown is shown in Figure 1(e). The charge disproportionation mode is analogous to the A-type anti-ferromagnetic configuration (hereafter Q_{ACD}) leads to a non-centrosymmetric $P4mm$ space group. Unlike Q_{GCD} , in Q_{ACD} the FeO_6 octahedra in a layer behave alike. This

arrangement of charge disproportionated mode reflects in FeO_6 octahedra which is in analogy with the A-type anti-ferromagnetic configuration and is shown in Figure 1(f). The Q_{ACD} mode appeared as imaginary frequency and alone exhibited a double well with small depth. Only coupling with the Q_{Tri} leads to a considerable double well indicating energy gain and strong coupling with Q_{Tri} , as shown in Figure 2(a).

We then examined how the charge disproportionation modes (i.e., Q_{GCD} , Q_{ACD}) which are individually responsible for the IMT are coupled to the other dominating distortions. As shown in Figure 2(b), among all the modes couplings, we have found that the coupling between Q_{Tri} and Q_{ACD} , i.e.; $Q_M \sim Q_{Tri} \otimes Q_{ACD}$ offers a polar Pc space group and ensures the lowest energy structure (30 meV/f.u. lower than $Pmc2_1$). Here, Q_M represents a multimode coupling term [20]. We have also considered a similar coupling between Q_{Tri} and Q_{GCD} and after geometry relaxation, it turned out that coupling between Q_{GCD} and Q_{Tri} is not stable. Here, to mention as shown in Figure 2(b), both Q_{Tri} and Q_{ACD} can lead to the respective non-centrosymmetric space groups.

In the presence of Q_{Tri} , $Pnma$ LaFeO_3 is an antiferromagnetic (G-type) insulator (d^5) and $Pnma$ CaFeO_3 is a ferromagnetic metal (d^4) (Supplementary Note: I). The magnetic ground state of $(\text{LaFeO}_3)_1/(\text{CaFeO}_3)_1$ superlattice within $Pmc2_1$ symmetry (i.e., in the presence of Q_{Tri}) is found to be C-type antiferromagnetic ordering with local magnetic moment on individual Fe is $3.81\mu_B$ indicating that Fe is in +4 charge state with d^4 electronic configuration. The missing of a hole per formula unit (f.u.) may be attributed to the phenomenon of ligand (O-2p) hole recombination [29]. Upon trilinear mode coupling in $(\text{LaFeO}_3)_1/(\text{CaFeO}_3)_1$ superlattice, the system is found to be metallic, and due to integration of Q_{ACD} the system emerged as a low bandgap semiconductor with an indirect energy bandgap of 0.28 eV, as shown in Figure 3 (a-b) within Pc space group. In Figure 3(a), the LB and SB represent long and short bonds between Fe and O-atoms, respectively, when the Q_{ACD} is coupled with Q_{Tri} . The appearance of LB and SB is a clear signature of charge disproportionation.

Analysis of the partial density of states (PDOS) and orbital projected DOS manifest that Fe-atoms interact antiferromagnetically, while O-2p and Fe-3d interaction is ferromagnetic type. This $p-d$ exchange gives rise to metallic phase due to Fe- e_g and O-2p within $Pmc2_1$, as shown in Figure (3)(c) (Supplementary Note: II). Contrary to the ligand-hole recombination for Q_{Tri} , in Q_M the system goes via a varying charge states solution. Here, Fe-atoms achieve two different moments, i.e.; $3.47\mu_B$ (Fe^{4+} oxidation state, d^4) and $4.05\mu_B$ (Fe^{3+} oxidation state, d^5) satisfying the oxidation of Fe in each block of the superlattice. In this case, the O-2p $_z$ and Fe-3d $_z$ hybridization is weak, and hence reduced moments are found on O-atoms. In addition, the Fe- e_g states pushed

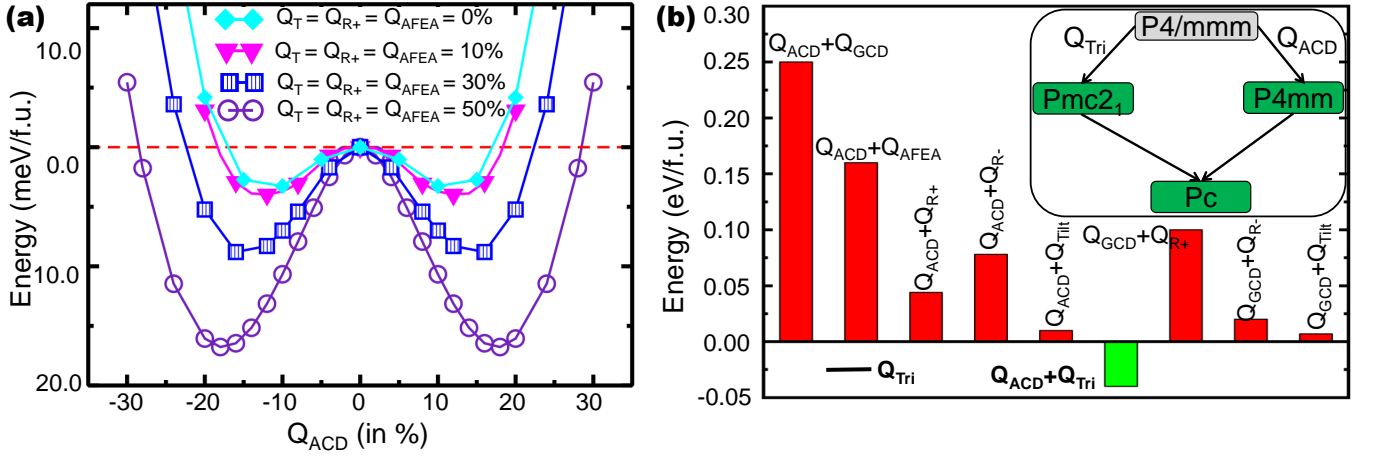


FIG. 2. (a) Evolution of energy in terms of Q_{ACD} mode amplitude with fixed amplitudes of Q_T , Q_{R+} , and Q_{AFEA} in the C-type antiferromagnetic ordering of $P4/mmm$ phase. (b) Comparative energetic bar diagram for various modes coupling with reference to the trilinear coupling term Q_{Tri} ; Inset: group-subgroup relationship for a multimode (Q_M) coupling, the space group highlighted with green represent non-centrosymmetric space group.

below the E_F and the system emerged as a semiconductor within space group Pc , as illustrated in Figure 3(c) (Supplementary Note: II for more details).

The question is now, how to modulate Q_M ? One possible way to "switch on" the modulation is to apply strain. Upon tensile and compressive strain, $(LaFeO_3)_1/(CaFeO_3)_1$ SL experiences a IMT. In the compressive region beyond 2.5% strain, the system is metallic while right from compressive 2.5% strain to tensile strain region the system behaves as a semiconductor, as shown in Figure 3(d). At compressive 2.5% strain, it shows a zero-band gap semiconducting phase, as shown in Figure 3(e). The electronic phase separation under strain is found to be a change in volume effect of the FeO_6 octahedra of the SL and the reconfiguration of t_{2g} and e_g is shown in Figure S5. The energy gap, E_g is found to be varying linearly with the change in volume, ΔV of the FeO_6 octahedra analogous to ref.[14] and is shown in Figure 3(f).

We fitted the Landau expansion [7, 13, 30], for the energy and obtained energy surface contour as a function of Q_{Tri} and Q_{ACD} (Supplementary Note: III for more details).

$$\begin{aligned}
 f(Q_{Tri}, Q_{ACD}) = & a_1 Q_{Tri}^2 + a_2 Q_{ACD}^2 + a_3 Q_{Tri}^2 Q_{ACD}^2 \\
 & + a_4 Q_{Tri}^4 + a_5 Q_{ACD}^4 + a_6 Q_{Tri}^6 + a_7 Q_{ACD}^6 \\
 & + a_8 Q_{Tri}^2 Q_{ACD}^4 + a_9 Q_{Tri}^4 Q_{ACD}^2 + a_{10} Q_{Tri}^8 \\
 & + a_{11} Q_{ACD}^8 + a_{12} Q_{Tri}^4 Q_{ACD}^4 + a_{13} Q_{Tri}^6 Q_{ACD}^2
 \end{aligned} \quad (1)$$

We found four equivalent minima with respect to the high symmetry $P4/mmm$ structure. The most energy gain is found when the amplitudes of both the modes are around $\sim 0.5 \text{ \AA}$ as shown in Figure 4(a). The coupling between Q_{Tri} and Q_{ACD} lowers the symmetry from metallic

$Pmc2_1$ to insulating Pc . The question is now how the coupling between Q_{Tri} and Q_{ACD} influences the polarization, magnetization, and density of states (DOS) at the E_F .

In Figure 4(b), utilizing the same expansion we have shown the variation of density of states at Fermi Level, i.e., $DOS@E_F$ as a function of (Q_{Tri}, Q_{ACD}) . The coupling between Q_{Tri} and Q_{ACD} gives rise to insulating and metallic regions. If we consider Q_{Tri} is fixed and switch the Q_{ACD} distortion in the opposite sense, i.e., from $-Q_{ACD} \rightarrow (Q_{ACD} = 0) \rightarrow +Q_{ACD}$, we can guide the system from insulating to metallic to again insulating phase. Contrarily, if one goes via Q_{Tri} mode, it is an insulating phase if Q_{ACD} gives an insulating solution and it is metal if Q_{ACD} is giving a metallic solution. The Q_{ACD} mode triggers the charge disproportionation which in turn makes the local magnetic moments on Fe atoms distinguishable by creating two different sublattices. In Figure 4(c), we have shown the difference in the magnetization i.e., ΔM , between +3 (d^5) and +4 (d^4) sublattices, as a function of Q_{Tri} and Q_{ACD} . The Q_{ACD} mode can reverse the sign of ΔM i.e., the two magnetic sublattices can be interchanged. The ΔM can be as large as $1.2\mu_B$ per f.u. depending on the strength of Q_{ACD} . When optimized to low symmetry Pc phase, the ΔM is found to be $0.58 \mu_B$ per f.u. Considering Figure 4(b) and (c), a clear correlation between $DOS@E_F$ and ΔM can be observed.

The Q_{AFEA} mode give rise to the finite polarization \mathbf{P} when La/Ca layered ordering has been established within $Q_M \sim Q_{Tri} \otimes Q_{ACD}$ and Q_{ACD} ensures an insulating phase. While varying the Q_{Tri} , we have first fixed the Q_{AFEA} at various magnitudes and by selective dynamics, Q_T and Q_R^+ distortions are allowed to relax. This establishes the fact that Q_{AFEA} (or Q_P) $\sim Q_{Tri}$. In

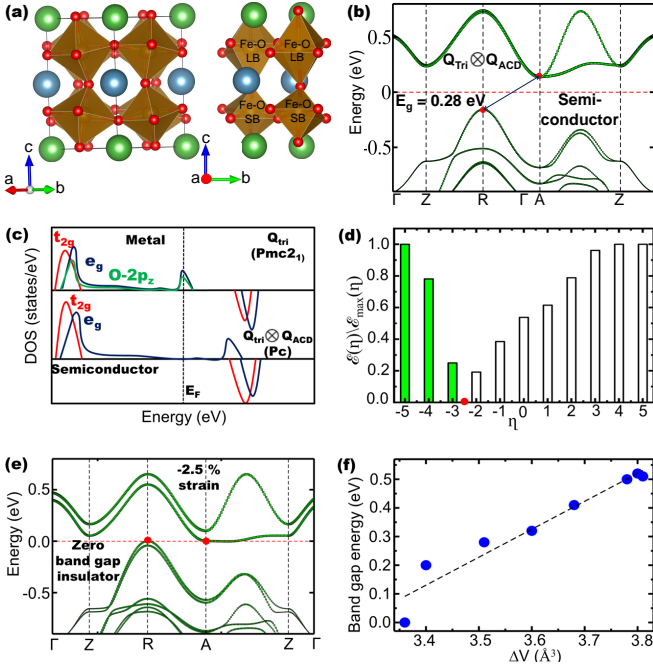


FIG. 3. (a) The lowest energy structure Pc . Here, LB and SB denote Fe-O long bond and short bond respectively. The green, blue, red, and golden balls represent La-, Ca-, O-, and Fe- atoms, respectively. (b) Band structure of Pc , (c) Illustration of insulator-to-metal transition using Crystal Field Splitting, (d) Variation of DOS@ E_F or Band Gap as a function of strain η . Here, $\xi(\eta)/\xi_{max}(\eta)$ is defined as the ratio between total DOS@ E_F and maximum total DOS@ E_F when the system is metallic (filled green), whereas, the same represents the ratio between band gap and maximum band gap when the system is insulating (empty). The negative sign indicates the compressive strain region, zero (0) denotes without any strain, and right to zero is the tensile strain region. (e) Band structure for zero-band gap insulating phase at compressive 2.5% strain. (f) The band gap energy is linearly varying with the change in volume, ΔV of the FeO_6 octahedra.

Figure 4(d) we have shown the variation of \mathbf{P} as a $f = (Q_{Tri}, Q_{ACD})$. When $Q_{ACD} = 0$, the polarization can not be measured as the system remains in the metallic region. But when both Q_{Tri} and Q_{ACD} mods are around $\sim 0.5 \text{ \AA}$, it shows a polarization as large as $40 \mu C/cm^2$ in the insulating phase. In the case of the optimized Pc phase, the total polarization is computed as $36.38 \mu C/cm^2$. Interestingly, we noticed that the directions of the polarization at four equivalent minima are different. This is due to the fact that both Q_{AFE} and Q_{ACD} are polar modes which give rise to the finite polarization along Cartesian y , P_y (crystallographic b) and z , P_z (Crystallographic c) directions, respectively. Along the Q_{AFE} (i.e., Q_{Tri}) the P_y can be reversed whereas along Q_{ACD} , P_z component can be reversed. The four polarization domains of (P_y, P_z) as $++$, $-+$, $+-$ and $--$ are possible considering coupling between Q_{Tri} and Q_{ACD} . Along the Q_{Tri} , only polarization switching can

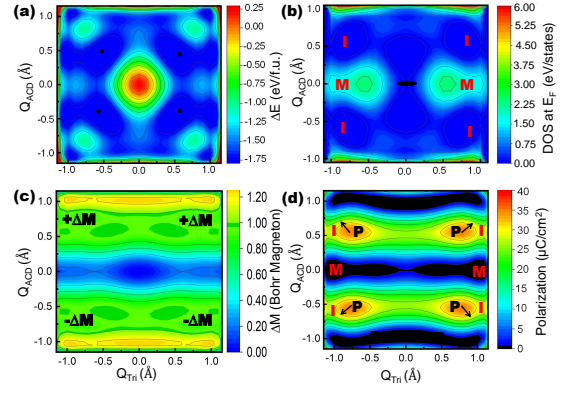


FIG. 4. (a) The energy surface contour plot as functions of Q_{Tri} and Q_{ACD} by using the Landau theory of phase transition. Subsequently, we have used the same equation for other physical properties to investigate the effect of various modes coupling; (b) density of states at the Fermi level (E_F), (c) change in magnetization due to Q_{ACD} , and (d) ferroelectric polarization from both Q_{Tri} and Q_{ACD} .

be observed. Interestingly, through Q_{ACD} system undergoes insulator-metal-insulator transition along with the polarization switching.

In $(LaFeO_3)_1/(CaFeO_3)_1$ SL, the emergent properties i.e., IMT, finite \mathbf{P} and \mathbf{M} and cross coupling between them depends on the strength of the coupling coefficients (i.e., a_i 's where $i=1,2,3 \dots$) as given in Equation 1. These coupling coefficients are materials specific but the effect is universal. To prove the concept of universality of multimode coupling, we have constructed artificial heterostructure superlattices of $(LaBO_3)_1/(CaB'O_3)_1$, where B in (+3 oxidation state) = $Cr(3d^3)$, $Mn(3d^4, e_g^1)$, $Fe(3d^5)$ and B' (in +4 oxidation state) = $Nb(4d^1, t_{2g}^1)$, $Mo(4d^2, t_{2g}^2)$ and $Ru(4d^4, e_g^1)$. We have started with the high symmetry $P4/mmm$ phase and invoke the trilinear coupling term Q_{Tri} into the system. A complete relaxation without symmetry constrain shows that the Q_{ACD} mode clubbing into the trilinear coupling term. This shows

TABLE I. Bandgap (B.G), polarization (P), and change in magnetization (ΔM) for $3d-4d$ $(LaBO_3)_1/(CaB'O_3)_1$ superlattices (SL). Here, M indicates metallic phase.

| $(LaBO_3)_1/(CaB'O_3)_1$ B(3d)/B'(4d) | B.G (eV) | P ($\mu C/cm^2$) | ΔM (μ_B) |
|--|-------------|-----------------------|---------------------------|
| Cr/Nb | M | M | 1.71 |
| Cr/Mo | 1.52 | 23.74 | 1.01 |
| Cr/Ru | 1.40 | 26.60 | 1.16 |
| Mn/Nb | M | M | 2.62 |
| Mn/Mo | 0.98 | 22.62 | 1.81 |
| Mn/Ru | 0.03 | 27.39 | 2.01 |
| Fe/Nb | M | M | 3.30 |
| Fe/Mo | 1.20 | 21.15 | 2.25 |
| Fe/Ru | 0.78 | 24.40 | 2.49 |
| $(LaFeO_3)_1/(CaFeO_3)_1$ | 0.28 | 36.38 | 0.58 |

universal coupling between Q_{Tri} and Q_{ACD} . The properties of $(LaBO_3)_1/(CaB'O_3)_1$ SLs are tabulated in Table I. All the Nb-based compounds are metallic whereas all the Mo- and Ru-based compounds are found to be insulating with band gap ranging from 0.03 eV - 1.52 eV, with maximum for $(LaCrO_3)_1/(CaMoO_3)_1$. Thus, we have identified both polar-metal and polar insulators with large ferroelectric (or, 'ferroelectric like' in the case of metals [20]) distortion. The change in ΔM follows a linear trend for a fixed $4d$ and for $(LaFeO_3)_1/(CaNbO_3)_1$ the value of ΔM is maximum as $3.5 \mu_B$. Total polarization values are found to be within the range of 21.5 - 27.39 $\mu C/cm^2$ and largest for $(LaMnO_3)_1/(CaRuO_3)_1$ heterostructure (polar vector Figure S7).

To conclude, we have proposed a mechanism of multi-mode coupling through which functional properties such as metal-to-insulator transition, polarisation and magnetization can be engineered at the $(LaFeO_3)_1/(CaFeO_3)_1$ oxide interface. The polarization is driven into the system by trilinear coupling Q_{Tri} , via Q_{AFEA} . The Q_{ACD} mode drives metal-to-insulator transition and polarization. By tuning the coupling between Q_{Tri} and Q_{ACD} , polar metallic phase, polar zero band gap semiconducting, and polar insulating phases can be obtained. The in-plane and out-of-plane polarization is induced into the system via Q_{AFEA} and Q_{ACD} distortions, respectively. Through Q_{ACD} path, the system undergoes insulator-metal-insulator transition along the polarization switching. The coupling mechanism between Q_{Tri} and Q_{ACD} and emergence of associated properties can be obtained for other superlattices with $Pnma$ building block and partially filled e_g or t_{2g} electron(s) at the B or B' sites.

M.S. acknowledges INSPIRE fellowship of Department of Science and Technology, New Delhi-110 016, Government of India. S.G. acknowledges DST-SERB Core Research Grant, File No. CRG/2018/001728 (2019-2022) for funding. M.S. and S.G. are grateful to SRM Institute of Science and Technology, Chennai, India for computational resources.

* saurabhghosh2802@gmail.com

- [1] W. Eerenstein, N. Mathur, and J. F. Scott, *nature* **442**, 759 (2006).
- [2] E. Bousquet, M. Dawber, N. Stucki, C. Lichtensteiger, P. Hermet, S. Gariglio, J.-M. Triscone, and P. Ghosez, *Nature* **452**, 732 (2008).
- [3] H. L. Boström, M. S. Senn, and A. L. Goodwin, *Nature communications* **9**, 1 (2018).
- [4] M. J. Pitcher, P. Mandal, M. S. Dyer, J. Alaria, P. Borisov, H. Niu, J. B. Claridge, and M. J. Rosseinsky, *Science* **347**, 420 (2015).
- [5] N. A. Benedek and C. J. Fennie, *Phys. Rev. Lett.* **106**, 107204 (2011).
- [6] S. Ghosh, H. Das, and C. J. Fennie, *Phys. Rev. B* **92**, 184112 (2015).
- [7] M. Shaikh, M. Karmakar, and S. Ghosh, *Phys. Rev. B* **101**, 054101 (2020).
- [8] J. M. Rondinelli and C. J. Fennie, *Advanced Materials* **24**, 1918 (2012).
- [9] M. Shaikh, A. Fathima, M. Swamynadhan, H. Das, and S. Ghosh, *Chemistry of Materials* **33**, 1594 (2021).
- [10] Y. S. Oh, X. Luo, F.-T. Huang, Y. Wang, and S.-W. Cheong, *Nature materials* **14**, 407 (2015).
- [11] F. Pomiro, C. Ablitt, N. C. Bristowe, A. A. Mostofi, C. Won, S.-W. Cheong, and M. S. Senn, *Phys. Rev. B* **102**, 014101 (2020).
- [12] G. Clarke, C. Ablitt, J. Daniels, S. Checchia, and M. S. Senn, *Journal of applied crystallography* **54** (2021), 10.1107/S1600576721001096.
- [13] A. Mercy, J. Bieder, J. Ñíguez, and P. Ghosez, *Nature communications* **8**, 1 (2017).
- [14] L. Jiang, D. Saldana-Greco, J. T. Schick, and A. M. Rappe, *Phys. Rev. B* **89**, 235106 (2014).
- [15] P. C. Rogge, R. U. Chandrasena, A. Cammarata, R. J. Green, P. Shafer, B. M. Lefler, A. Huon, A. Arab, E. Arenholz, H. N. Lee, T.-L. Lee, S. Nemšák, J. M. Rondinelli, A. X. Gray, and S. J. May, *Phys. Rev. Materials* **2**, 015002 (2018).
- [16] G. M. Dalpian, Q. Liu, J. Varignon, M. Bibes, and A. Zunger, *Phys. Rev. B* **98**, 075135 (2018).
- [17] D. Preziosi, L. Lopez-Mir, X. Li, T. Cornelissen, J. H. Lee, F. Trier, K. Bouzehouane, S. Valencia, A. Gloter, A. Barthélémy, *et al.*, *Nano letters* **18**, 2226 (2018).
- [18] C. Domínguez, A. B. Georgescu, B. Mundet, Y. Zhang, J. Fowlie, A. Mercy, A. Waelchli, S. Catalano, D. T. Alexander, P. Ghosez, *et al.*, *Nature Materials* **19**, 1182 (2020).
- [19] Y. Zhang, M. M. Schmitt, A. Mercy, J. Wang, and P. Ghosez, *Phys. Rev. B* **98**, 081108 (2018).
- [20] S. Ghosh, A. Y. Borisevich, and S. T. Pantelides, *Phys. Rev. Lett.* **119**, 177603 (2017).
- [21] P. C. Rogge, R. J. Green, P. Shafer, G. Fabbris, A. M. Barbour, B. M. Lefler, E. Arenholz, M. P. M. Dean, and S. J. May, *Phys. Rev. B* **98**, 201115 (2018).
- [22] M. Shaikh, M. Karmakar, and S. Ghosh, *Physical Review B* **101**, 054101 (2020).
- [23] P. Hohenberg and W. Kohn, *Phys. Rev.* **136**, B864 (1964).
- [24] R. D. King-Smith and D. Vanderbilt, *Phys. Rev. B* **47**, 1651 (1993).
- [25] G. Kresse and J. Furthmüller, *Phys. Rev. B* **54**, 11169 (1996).
- [26] V. I. Anisimov, F. Aryasetiawan, and A. Lichtenstein, *Journal of Physics: Condensed Matter* **9**, 767 (1997).
- [27] S. L. Dudarev, G. A. Botton, S. Y. Savrasov, C. J. Humphreys, and A. P. Sutton, *Phys. Rev. B* **57**, 1505 (1998).
- [28] J. P. Perdew, A. Ruzsinszky, G. I. Csonka, O. A. Vydrov, G. E. Scuseria, L. A. Constantin, X. Zhou, and K. Burke, *Phys. Rev. Lett.* **100**, 136406 (2008).
- [29] E. Cho, K. Klyukin, S. Ning, J. Li, R. Comin, R. J. Green, B. Yildiz, and C. A. Ross, *Physical Review Materials* **5**, 094413 (2021).
- [30] N. Sivadas, P. Doak, and P. Ganesh, *arXiv preprint arXiv:2106.08783* (2021).